# $N_2O$ Adsorption and Photochemistry on Ceria Surfaces

Chengwu Yang,* Yunjun Cao, Philipp N. Plessow, Jia Wang, Alexei Nefedov, Stefan Heissler, Felix Studt, Yuemin Wang, Hicham Idriss, Thomas G. Mayerhöfer, and Christof Wöll*

**ABSTRACT:** Catalytic decomposition of nitrous oxide ($N_2O$) is one of the most promising ways to control $N_2O$ emissions, the dominant ozone depleting substance and the third most potent greenhouse gas. We have investigated the adsorption and photoinduced decomposition of $N_2O$ on macroscopic monocrystalline $CeO_2(111)$ surfaces by polarization dependent infrared reflection absorption spectroscopy (IRRAS) in conjunction with core level (XPS Ce 3d and NEXAFS) and valence band (Ce 4f) spectroscopy as well as DFT+U calculations. The IRRAS results at 110 K show that the $\nu_{as}$(NNO) asymmetric stretching vibration of adsorbed $N_2O$ exhibits band splitting at relatively low $N_2O$ coverage in p polarized spectra. This band splitting is attributed to polarization dependent shifts of absorption bands. On reduced ceria (111) surfaces, the desorption energy (0.37 eV) of $N_2O$ extracted by IRRAS is found to be higher than on oxidized surfaces. This increasing binding energy is attributed to the attractive coupling with $Ce^{3+}$ cations formed via surface $Ce^{4+}$ reduction by by polarons that migrate from the bulk. The photoreaction cross section (with ultraviolet (UV) light = 365 nm at $T$ = 120 K) of the reduced ceria (110) surfaces determined by IRRAS ($5 \times 10^{-19}$ $cm^2$) confirms their much higher activity than that of the reduced $CeO_2(111)$.

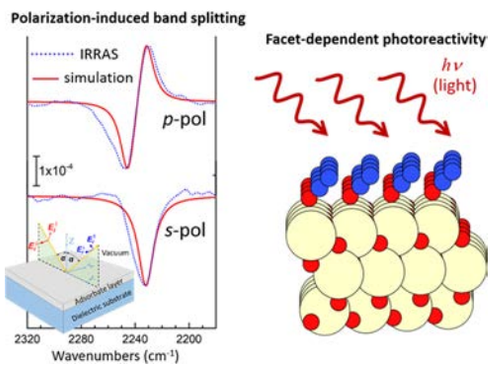


## 1. INTRODUCTION

Ceria ($CeO_2$) is one of the most studied oxide supports in catalysis for a large number of technically important chemical reactions.[1−3] Its high catalytic activity and stability, especially for redox reactions, are related to the ease of its reduction and the associated lattice oxygen transfer for oxidation reactions. Complementing the catalytic cycle, the then formed O vacancies ($V_O$) are healed either in an oxygen rich environ ment or by an oxygen containing compound (Mars−van Krevelen mechanism).[4] Ceria has also been found to act as a photocatalyst,[5−9] although its band gap (O 2p → Ce 5d) is large (about 6 eV).[10−14] This has been attributed to the O 2p → Ce 4f transition, which lies in about the middle of the O 2p → Ce 5d transition. In a previous work, we have shown that the reduced ceria (110) single crystal surface exhibited high photoexcited activity, using the photodecomposition of nitrous oxide ($N_2O$) as a prototype oxygen containing reactant.[15] The photoactivation of ceria is attributed to the filling of these mid gap states upon the creation of surface oxygen vacancies, resulting in two undercoordinated $Ce^{3+}$ sites per oxygen atom removed from the lattice. This is one of a few photochemical studies on oxide single crystal surfaces performed to date in the surface science of model oxide semiconductors.[16,17]

The process of $N_2O$ decomposition is of global environ mental importance as $N_2O$ is now the most significant ozone depleting compound in the atmosphere[18] as well as the third most important greenhouse gas in terms of radiative forcing.[19] Moreover, global $N_2O$ emissions are accelerating (at present it is in the $10^6$ ton N/year range,[20] mostly from agricultural sources).[21] Because $N_2O$ is a stable molecule that lasts over 100 years in the troposphere, it would continue to contribute to ozone depletion (upper atmosphere), if not curbed, and undermine the achievements of the Montreal Protocol.[22,23]

Because of the relative inertness of the $N_2O$ molecule,[24] high temperature catalytic reactions are required for a kinetically relevant thermal decomposition of the N−O bond.[25] Light excitation, may then prove to be useful for the decomposition of $N_2O$ either to replace the thermal process or to act in synergism with it (photothermal).[26−29] The overall reaction in its thermal or photoexcited catalytic pathway is the following: $N_2O \rightarrow N_2 + 1/2\ O_2$, which has been studied catalytically on a few catalysts including ZnO, $TiO_2$, and $CeO_2$.[30−32]

In this work, we address the nature of interaction of $N_2O$ over model $CeO_2$ surfaces in their stoichiometric and reduced states to see for possible structure sensitivity effects on its mode of adsorption using infrared reflection absorption spectroscopy (IRRAS). The work is complemented by core level (X ray photoelectron spectroscopy (XPS) and near edge

X ray absorption fine structure (NEXAFS) spectroscopy) and valence band photoemission spectroscopy (VB PES) as well as computationally using DFT+U. The overall objective is to gain fundamental knowledge and to extract reliable experimental parameters that can be transferred to catalysis to help increase their activity either thermally or upon illumination.

## 2. METHODS

**2.1. IRRAS, XPS, Low-Energy Electron Diffraction (LEED), and UV Irradiation Experiments.** IRRAS measurements were performed in a ultrahigh vacuum (UHV) apparatus combining a state of the art FTIR spectrometer (Bruker Vertex 80v) with a multichamber UHV system (Prevac).[33] The $CeO_2$ single crystals (SurfaceNet) were prepared by repeated cycles of sputtering with 1 keV $Ar^+$ and annealing at 800 K for 15 min in an $O_2$ atmosphere of $1 \times 10^{-5}$ mbar to form a fully oxidized surface, or alternately without $O_2$ to create oxygen vacancies on the surface.[34−36] Low energy electron diffraction (LEED) (OCI Vacuum Microengineering BDL800) was used to ensure a well defined surface crystallinity of the substrate, which can be judged by the sharp spots in the LEED pattern. In addition, X ray photoelectron spectroscopy (XPS) measurements in grazing emission geometry were carried out to ensure the cleanliness of the sample and to determine the oxidation state of cerium from Ce 3d photoemission spectra prior to IRRAS measurements.[36] Exposure to $N_2O$ at sample temperatures typically below 120 K was achieved by backfilling the IR chamber with a leak valve based directional doser connected to a tube (2 mm in diameter) that terminated 3 cm from the sample surface and 50 cm from the hot cathode ionization gauge. The base pressure during the acquisition of IR spectra was $\sim 8 \times 10^{-11}$ mbar. The IR spectra were recorded with p and s polarized light. UV irradiation was performed with a 365 nm LED and the UV light fell on the sample through a quartz window in the UHV chamber. The light flux was determined to be 0.5 mW·$cm^{-2}$ or $9.2 \times 10^{14}$ photons·$s^{-1}$·$cm^{-2}$.

**2.2. Density Functional Theory Computation (DFT).** Periodic DFT calculations were carried out with the projector augmented wave (PAW) method using the VASP program package in version 5.4 as well as the standard VASP PAWs.[37,38] The Brillouin zone was sampled with a Γ centered k point grid and a $4 \times 4$ mesh for the $1 \times 1$ unit cell of $CeO_2(111)$ and equivalent $k$ points for larger supercells. A Gaussian smearing with a width of 0.1 eV was used. An energy cutoff of 400 eV was used for the expansion of the wave function in the plane wave basis set and 800 eV if the volume of the unit cell was changed in the optimization of cells. The obtained length of the lattice vectors of the unit cell of bulk $CeO_2$ is 5.472 Å. Slabs of the surfaces were separated by ∼16 Å to prevent artificial interaction between the slabs. The PBE functional with Grimme's correction (PBE D3) was used in all calculations,[39−41] along with a Hubbard U correction in the formulation by Dudarev[42−45] ($U$ = 5 eV), abbreviated as PBE D3+U. As one would expect, the Hubbard correction has no significant effect on the calculations of stoichiometric $CeO_2$. Harmonic force constants have been obtained from a central finite difference scheme with an offset of 0.1 Å. In these calculations, the adsorbed $N_2O$ and the top Ce layer were included. Generally, the effect of including parts of the $CeO_2$ surface was found to be negligible.

**2.3. VB-PES Experiments.** NEXAFS and VB PES experiments were carried out on the HESGM beamline at Helmholtz Zentrum Berlin (HZB).[46] VB PES spectra were measured to determine the oxidation state of cerium. It is worth noting that the electrical conductivity of bulk ceria is quite low and decreases even more with decreasing temperature. At temperatures below 150 K, the charging effect becomes so strong that VB PES experiments were no longer possible. Therefore, VB PES spectra were recorded at sample temperatures above 150 K. We measured $CeO_2$ (with different surface orientations) many times and never detected visible reduction of ceria during X ray irradiation.

NEXAFS data were acquired in the partial electron yield (PEY) mode at an incident angle of 55° with linearly polarized light. Fortunately, NEXAFS spectroscopy is not affected by the charging problem that greatly hinders VB PES measurements at low temperatures. Therefore, measurements were carried out at the N K edge directly after $N_2O$ exposure at 120 K. Raw spectra were analyzed according to the following procedure: First, a NEXAFS spectrum measured for clean $CeO_2$ was subtracted from the ones recorded after $N_2O$ exposure to exclude the unwanted contribution of the $CeO_2$ substrate. Subsequently, the data were divided by a spectrum of a freshly sputtered Au wafer to account for the energy dependence of the direct beam and to compensate for carbon contamination of the beamline optics.[14]

$N_2O$ exposure was achieved by backfilling the chamber up to $10^{-9}$ mbar at a sample temperature of 120 K. The typical base pressure during the acquisition of NEXAFS and VB PES spectra was $2 \times 10^{-10}$ mbar. After $N_2O$ exposure, NEXAFS and VB PES spectra were recorded at 120 and 250 K for NEXAFS and VB PES, respectively.

## 3. RESULTS AND DISCUSSION

**3.1. Coverage Effect.** Figure 1 shows the polarization resolved IRRA spectra recorded after exposure of the fully oxidized $CeO_2(111)$ surface to 5 Langmuir (L) of $N_2O$ at 110 K. In the p polarized spectrum, a positive band is observed at 2232 $cm^{-1}$ and a negative band at 2255 $cm^{-1}$, while in the s polarized spectrum only a negative band is seen at 2234 $cm^{-1}$. As a result of optical effects, the signals in the p polarized spectrum are about three times larger than in the corresponding s polarized spectrum. These bands all originate

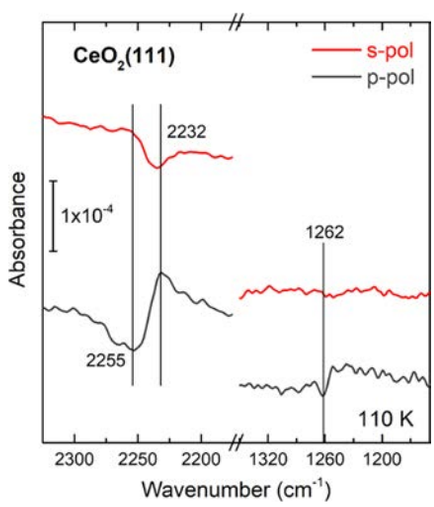


**Figure 1.** IRRA spectra of the oxidized $CeO_2(111)$ surface exposed to 5 L of $N_2O$ at 110 K with p and s polarized light.

from the asymmetric stretching vibration ($\nu_{as}$) of the adsorbed $N_2O$ molecules and are blue shifted compared to the gas phase value (2224 $cm^{-1}$). The symmetric stretching vibration ($\nu_s$) of the adsorbed $N_2O$ molecules leads to a single peak at 1262 $cm^{-1}$ in the p polarized spectrum, which is red shifted with respect to the gas phase $\nu_s$(NNO) = 1285 $cm^{-1}$. We note that the much lower intensity of the $\nu_s$(NNO) bands for s polarized light hinders observation, and the peak is below the noise level.

With regard to molecules adsorbed on a dielectric surface, the sign of the IR absorption bands is related to the orientation of the responsible transition dipole moment (TDM).[33,47−49] For p polarized light, positive absorption bands arise from the vibrations that have a component of the TDM parallel to the surface, while negative absorption bands are caused by the vibrations having a component perpendicular to the surface. Accordingly, the positive band corresponds to the in plane $N_2O$ vibrational mode and the negative one to the out of plane vibrational mode. For s polarized light, absorption bands are always negative and are nonzero only when the component of the molecular vibration is parallel to the s polarized light. Based on the polarization dependent IRRAS data shown in Figure 1 and the findings of previous studies,[28,50−53] we conclude that $N_2O$ species are bound to surface Ce cations via the O end in a tilted geometry.

To better understand the vibrational frequency and geometry of the adsorbed $N_2O$ molecules on the oxidized $CeO_2$(111) surface, we performed first principles DFT calculations (Figure 2 and Table 1). DFT calculations confirm the presence of a tilted adsorption geometry, with the $N_2O$ species bound via the O end to regular 7 fold coordinated surface $Ce^{4+}$ sites. Depending on the coverage, the tilt angle decreases from 74° at 0.25 monolayer (ML) to 44° at full ML (the normal to surface = 0°, Figure 2). We note that the calculated adsorption energies are comparable for the O bound and N bound $N_2O$ molecules. However, the calculated vibrational frequencies for the O end configuration are in better agreement with the experimental IRRAS data than the N end configuration (Table 1).

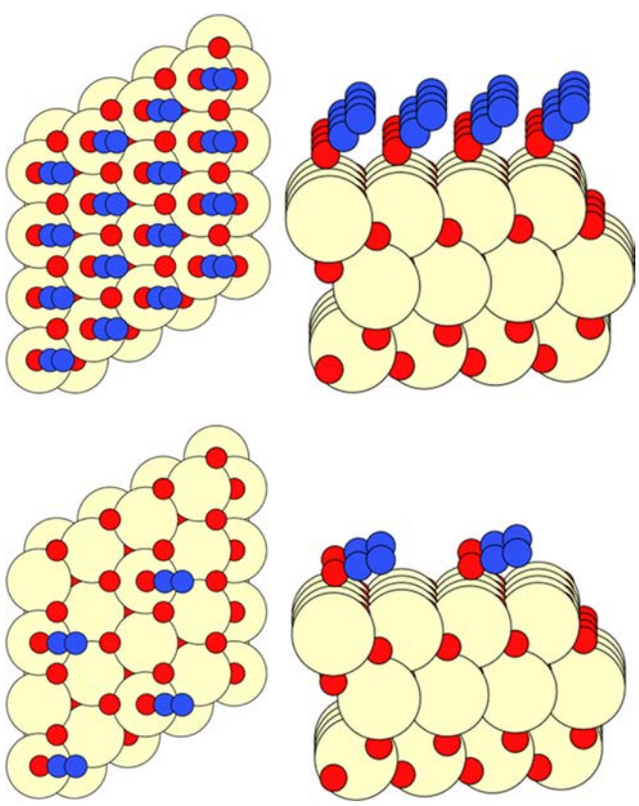

**Figure 2.** Top and side view of O bound $N_2O$ on the $CeO_2$(111) surface at a coverage of 1 ML (top) and 0.25 ML (bottom) for DFT optimized structures.

After annealing at 800 K under UHV conditions (in the absence of $O_2$), a reduced $CeO_{2-x}$(111) surface was obtained. Figure 3a shows p polarized IRRAS results obtained after $N_2O$ adsorption on the reduced $CeO_{2-x}$(111) surface at 110 K. At low coverage, i.e., low dosage (0.01 L $N_2O$), a single band is observed at 2244 $cm^{-1}$ in the $\nu_{as}$(NNO) region. When the $N_2O$ dosage is increased to 0.05 L, a negative band at 2260 $cm^{-1}$ shows up in addition to the positive band, which shifts to 2236 $cm^{-1}$. As the $N_2O$ dosage is further increased, these two bands gradually shift to lower frequencies, accompanied by an increase in absorption intensity. At saturation adsorption of $N_2O$, the positive and negative bands shift to 2231 and 2248 $cm^{-1}$, respectively. We attribute these coverage dependent shifts mainly to a combination of dynamic dipole coupling and substrate mediated chemical interactions.[54] Figure 3b shows the s polarized IRRAS results obtained after $N_2O$ adsorption on the reduced $CeO_{2-x}$(111) surface. At low coverage, only one negative band is observed at 2244 $cm^{-1}$, which shifts to 2232 $cm^{-1}$ at saturation coverage. The corresponding symmetric $\nu_s$(NNO) band appears at ∼1260 $cm^{-1}$ for both p and s polarized light (not shown). As shown in Figure 3c, the s polarized light signal, while weaker than the p polarized one, tracks better the surface coverage, with virtually no change in signal intensity or in frequency between the 2 and 5 L exposures and indicates a sticking coefficient near unity at this temperature (110 K).

**3.2. Temperature Effect: Adsorption at 110 K.** Figure 4a shows the temperature dependent signal of the asymmetric stretching vibrations of $N_2O$ adsorbed on fully oxidized $CeO_2$(111) single crystal surfaces. The positive and negative bands decrease in intensity simultaneously and disappear completely at about 125 K. In comparison, the vibrational bands of $N_2O$ molecules adsorbed on the reduced $CeO_{2-x}$(111) surface (see Figure 4b) are three times higher in intensity than those of the oxidized $CeO_2$(111) surface. The corresponding species are also more stable, with their bands disappearing at about 20 K higher temperatures (145 K).[50] The intensities of positive and negative bands also decrease in a simultaneous mode with increasing temperature. There is a general consensus that for ceria (111), subsurface vacancies are more stable than the surface ones, and the excess electrons are preferably located at Ce cationic sites of the outermost cationic plane, rather than in deeper layers.[55−60] These excess electrons occupy the Ce 4f electronic states within the band gap (O 2p−Ce 5d), thus leading to the formation of small polarons. The activation barrier for hopping of the polarons is below 0.5 eV.[61−64] We propose that after adsorption of the $N_2O$ molecules, the polarons diffuse to the Ce cations on the surface and the resulting $Ce^{3+}$ interacts with the adsorbed molecules, leading to a higher binding energy on the reduced ceria (111) surface compared to the oxidized one, as confirmed by the temperature resolved IRRAS data (Figure 4). Assuming a first order desorption and a preexponential factor of $10^{13}$ $s^{-1}$, the activation energy for $N_2O$ desorption ($E_d$) could be determined based on a quantitative analysis of the IR data

**Table 1. Calculation Results of $N_2O$ Adsorption on Oxidized $CeO_2(111)$ Surfaces**

| bond mode | coverage (ML) | supercell | $\nu_s(N_2O)^a$ (cm) | $\nu_{as}(N_2O)^a$ (cm) | tilt angle$^b$ (deg) | $E_{ads}$ (eV) | structure |
|---|---|---|---|---|---|---|---|
| O-bound | 1 | 1 × 1 | 1285 | 2237 | 44 | 0.28 | Figure 2 |
| | 0.25 | 2 × 2 | 1273 | 2228 | 74 | 0.25 | Figure 2 |
| N-bound | 1 | 1 × 1 | 1294 | 2249 | 39 | 0.30 | Figure S1 |
| | 0.25 | 2 × 2 | 1293 | 2226 | 79 | 0.22 | Figure S2 |

$^a$The computed frequencies of $\nu_s(N_2O)$ and $\nu_{as}(N_2O)$ for adsorbed $N_2O$ were corrected by the experimental values (1285 and 2224 $cm^{-1}$) and computed values (1323.5 and 2349.0 $cm^{-1}$) of $\nu_s(N_2O)$ and $\nu_{as}(N_2O)$ for gas phase $N_2O$, i.e., all computed frequencies were multiplied by the ratio of the experimental to computed value for gas phase $N_2O$ for $\nu_s(N_2O)$ and $\nu_{as}(N_2O)$, respectively. $^b$Tilt angle nomenclature: upright = 0°, completely horizontal = 90°.

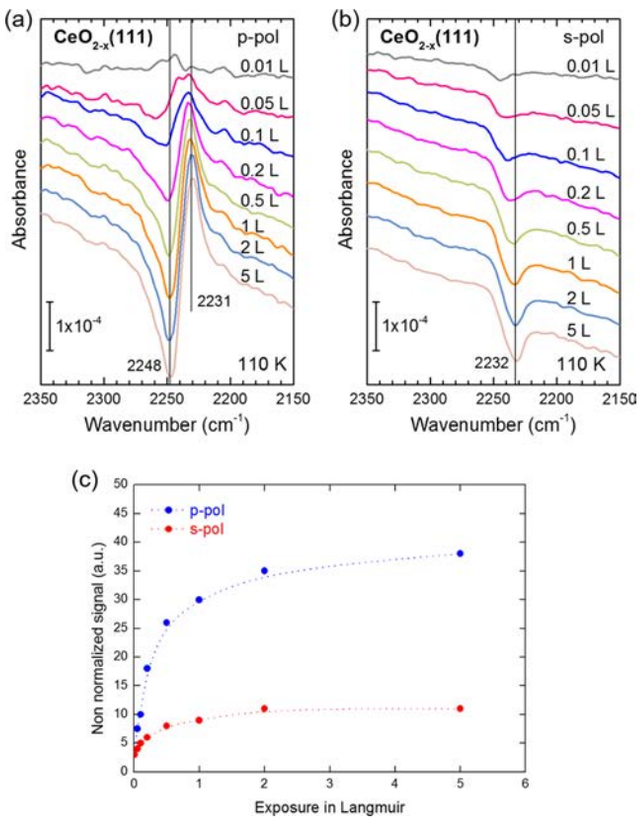


**Figure 3.** IRRA spectra of $N_2O$ adsorbed on reduced $CeO_{2-x}(111)$ as a function of $N_2O$ dosage at 110 K with (a) p and (b) s polarized light. (c) Integrated signals for p and s polarized light as a function of $N_2O$ dosage.

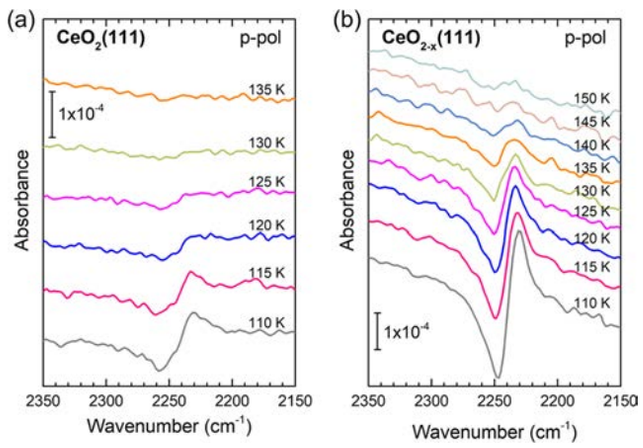


**Figure 4.** IRRA spectra recorded in situ after exposing ceria surfaces to 5 L $N_2O$ at 110 K with p polarized light (lowest trace) and then heating gradually up to the indicated temperatures. (a) $N_2O$ on the fully oxidized $CeO_2(111)$ surface and (b) $N_2O$ on the reduced $CeO_{2-x}(111)$ surface.

(Figures S3 and S4). These are estimated to be equal to 36 kJ $mol^{-1}$ (0.37 eV) and 33 kJ $mol^{-1}$ (0.34 eV) for the reduced and stoichiometric surfaces, respectively. The adsorption energies computed using DFT+U (Table 1) gave an adsorption energy of $N_2O$ on the oxidized $CeO_2(111)$ close to the desorption energy extracted experimentally: 0.25−0.28 eV (at coverages of 0.25 and 1 ML).[65]

Weiss[66] and Heidberg et al.[67] investigated the adsorption of $N_2O$ molecules on NaCl(001) and MgO(001) single crystal surfaces by polarization dependent infrared spectroscopy in a transmission mode and detected a pair of absorption peaks in the $\nu_{as}$(NNO) region, which they attributed to correlation field splitting (or Davydov splitting) caused by the coupling of the transition dipole moment between neighboring molecules within the adsorbate layer.[66,67] The resulting absorption doublet consists of a symmetric (in phase) and an asymmetric (out of phase) line with different frequencies. However, the correlation field splitting in IR spectra has been observed for these systems only upon the formation of a densely packed, ordered $N_2O$ layer (a two dimensional crystal) at very low temperatures. Since in our case, the splitting already occurs at the initial $N_2O$ adsorption and the two coupled vibrational modes evolve synchronously until saturated adsorption, the crystal field splitting can be excluded in this case. Instead, we propose that the splitting of the vibrational modes results from polarization dependent shifts of the absorption bands.[68] For CO adsorbed on $CeO_2(111)$ these shifts are rather small (4 $cm^{-1}$), but for $N_2O$ the transition dipole moment is substantially larger, leading to larger shifts. In ref 68, we modeled this so called Berreman effect[69] by assuming a monolayer film with an effective dielectric function using a transfer matrix approach to calculate the reflectance. The dielectric function tensor (for details see ref 68) was generated by assuming the classical damped harmonic oscillator model with one oscillator having the parameters $S$ = 800 $cm^{-1}$ (oscillator strength), $\gamma$ = 14 $cm^{-1}$ (damping constant), and $\tilde{\nu}_0$ = 2232 $cm^{-1}$. The tilt angle was assumed to be 64° relative to the surface normal. The simulations using these input parameters reproduce the experimental spectra remarkably well, see Figure 5. Note that the adjustable parameters in these simulations, the oscillator parameters and the tilt angle, were only estimated, but not optimized and all other parameters were obtained from the known optical parameters of $CeO_2$. We thus conclude that the occurrence of a single negative peak in the s polarized spectrum, a negative, and a positive peak in the p polarized spectrum as well as the relative intensities are fully consistent with the simulations. We also note that a TO−

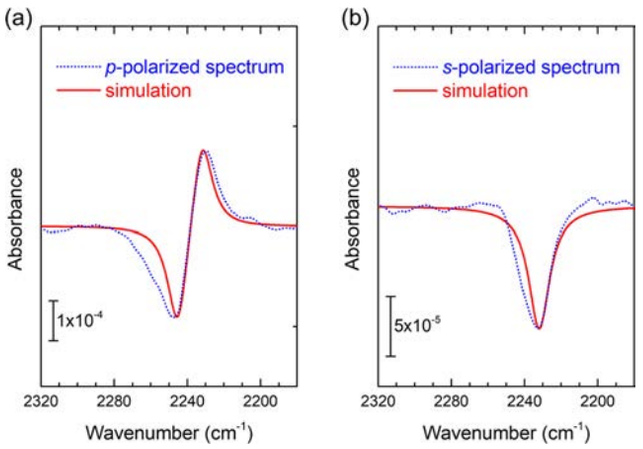


**Figure 5.** Comparison of simulated data $A_{p,sim} = -\lg(R_p/R_{0p})$ and $A_{s,sim} = -\lg(R_s/R_{0s})$ (solid lines) with experimental data for $N_2O$/$CeO_2(111)$ $A_{p,exp}$ and $A_{s,exp}$ (dotted lines) are shown in panels (a) and (b), respectively.

LO splitting of about 15 $cm^{-1}$ in the p polarized data agrees with literature values.[70]

**3.3. Adsorption at 78 K.** Figure 6 shows the p polarized spectra of $N_2O$ adsorbed on the oxidized $CeO_2(111)$ surface as

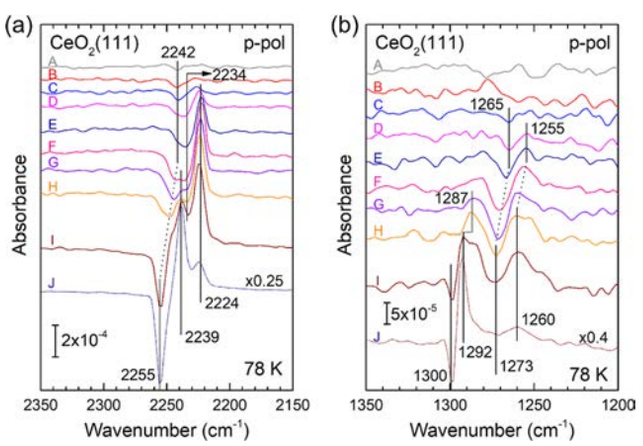


**Figure 6.** IRRA spectra of $N_2O$ adsorbed on oxidized $CeO_2(111)$ as a function of $N_2O$ dosage at 78 K with p polarized light. (a) Region of $\nu_{as}$(NNO) bands and (b) region of $\nu_s$(NNO) bands. The exposures in units of Langmuir are (A) 0.02, (B) 0.05, (C) 0.07, (D) 0.1, (E) 0.2, (F) 0.5, (G) 0.7, (H) 1.0, (I) 2.0, and (J) 5.0.

a function of $N_2O$ dosage at 78 K. At an $N_2O$ dosage of 0.02 L, the spectrum in the $\nu_{as}$(NNO) region consists of a single negative peak at 2242 $cm^{-1}$ (Figure 6a). At an $N_2O$ dosage of 0.05 L, another negative peak appears at 2234 $cm^{-1}$, which grows with increasing $N_2O$ dosage. Simultaneously, a positive peak appears at 2224 $cm^{-1}$, which nearly matches the $\nu_{as}$ value of $N_2O$ in the gas phase and continues to grow as the $N_2O$ dosage increases. The close proximity to the gas phase $\nu_{as}$(NNO) frequency is a coincidence, since we can rule out that gas phase $N_2O$ is present in these experiments. Interestingly, when the $N_2O$ dosage reaches 1 L, a new positive peak at 2239 $cm^{-1}$ and a negative one at 2255 $cm^{-1}$ show up and dominate the spectra at higher $N_2O$ dosages. These two bands do not saturate in intensity and are thus assigned to $N_2O$ multilayer species. In the symmetric $\nu_s$(NNO) region (Figure 6b), a doublet appears at 1265 (negative) and 1255 $cm^{-1}$ (positive) at low coverages and gradually shifts to 1273/1260 $cm^{-1}$ with increasing $N_2O$ dosage. At $N_2O$ dosage above 0.7 L, an additional doublet at 1300 (negative) and 1292 $cm^{-1}$ (positive) develops into the dominant bands, revealing the formation of $N_2O$ multilayers.

Figure 7 shows the s polarized spectra of $N_2O$ adsorbed on the oxidized $CeO_2(111)$ surface at 78 K as a function of $N_2O$

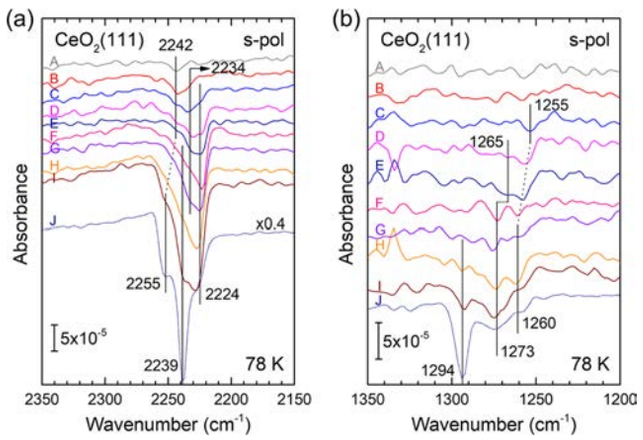


**Figure 7.** IRRA spectra of $N_2O$ adsorbed on oxidized $CeO_2(111)$ as a function of $N_2O$ dosage at 78 K with s polarized light. (a) Region of $\nu_{as}$(NNO) bands and (b) region of $\nu_s$(NNO) bands. The exposures in units of Langmuir are (A) 0.02, (B) 0.05, (C) 0.07, (D) 0.1, (E) 0.2, (F) 0.5, (G) 0.7, (H) 1.0, (I) 2.0, and (J) 5.0.

coverage. At an $N_2O$ dosage of 0.02 L, the spectrum in the $\nu_{as}$(NNO) region consists of a single peak at 2242 $cm^{-1}$, which gradually shifts to 2224 $cm^{-1}$ with increasing $N_2O$ coverage. As the $N_2O$ dosage reaches 1.0 L, a new band at 2239 $cm^{-1}$ appears and becomes the dominant one at higher $N_2O$ coverages. In the $\nu_s$(NNO) region, the spectra are dominated by a band at 1255 $cm^{-1}$ that shows a blue shift to 2160 $cm^{-1}$ with increasing $N_2O$ coverage (Figure 7b). For dosage higher than 1.0 L, a negative peak emerges at 1294 $cm^{-1}$ and dominates the spectrum at the highest $N_2O$ dosage (5.0 L).

Clearly, the evolution of $N_2O$ bands in p polarized spectra is in sync with that in s polarized spectra. The intensity of these bands monitors the process of $N_2O$ adlayer formation, starting with a sub monolayer to a full monolayer and finally $N_2O$ multilayers. Overall, the splitting of the vibrational modes of the adsorbed $N_2O$ molecules is also detected for p polarized spectra in the monolayer regime at 78 K. Furthermore, this polarization induced splitting leads to the appearance of a negative peak at a higher frequency and a positive peak at a lower frequency, in line with the spectra acquired at higher temperatures (110 K). We would like to emphasize that at 78 K, the polarization dependent band splitting is observed for both $\nu_{as}$(NNO) and $\nu_s$(NNO) vibrations in p polarized spectra (Figure 6). Considering that the oxidized $CeO_2(111)$ surface is almost free of defects, as suggested by surface ligand IR (SLIR) spectroscopy[71] and carbon monoxide (CO) adsorption,[55] the presence of defect related $N_2O$ species can be ruled out. Importantly, we also see the band splitting in p polarized spectra for $N_2O$ multilayers (Figure 6). The doublets in both $\nu_{as}$(NNO) and $\nu_s$(NNO) regions are attributed to the coupling of the fundamental vibrational modes to longitudinal optical (LO) and transversal optical (TO) phonons in $N_2O$ multilayers.[70] The observation of sharp LO (negative bands) and TO (positive bands) peaks indicates the formation of

ordered, polarized $N_2O$ thin films on ceria surfaces at 78 K. Table 2 shows the mode assignments of the observed vibrational bands in p and s polarized spectra.

**Table 2. Vibrational Frequencies ($cm^{-1}$) and Mode Assignments of $N_2O$ Adsorption on Oxidized $CeO_2(111)$ Surfaces at 78 K**

| | $\nu_{as}(N_2O)$ | | $\nu_s(N_2O)$ | |
|---|---|---|---|---|
| coverage | p-*pol* | s-*pol* | p-*pol* | s-*pol* |
| sub-monolayer | 2242 | 2242 | 1265/1255 | 1255 |
| monolayer | 2234/2224 | 2224 | 1273/1260 | 1260 |
| multilayers | 2255/2239 | 2239 | 1300/1292 | 1294 |

**3.4. Temperature Effect: High Exposure at 78 K.** Figure 8 shows the infrared spectra recorded after multilayer

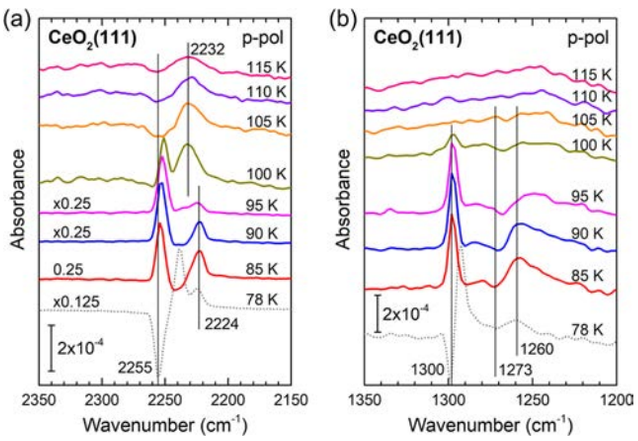


**Figure 8.** IRRA spectrum recorded directly after exposing the oxidized $CeO_2(111)$ to 5 L $N_2O$ at 78 K with p polarized light (lowest trace) and then heating gradually up to the indicated temperatures.

adsorption of $N_2O$ (5 L) onto the oxidized $CeO_2(111)$ surface at 78 K with p polarized light (lowest trace) followed by heating gradually up to the indicated temperatures. When the temperature is raised to 85 K, the characteristic doublet at 2255/2239 $cm^{-1}$ for $N_2O$ multilayers cannot be detected anymore, while a positive peak at 2253 $cm^{-1}$ shows up. The latter one undergoes a slight red shift with increasing temperature and totally disappears upon heating to 105 K. In the $\nu_s$(NNO) region, the corresponding vibrations at 1300 and 1292 $cm^{-1}$ show a similar behavior. Both multilayer $N_2O$ related peaks are replaced by a positive one at 1298 $cm^{-1}$ that disappears only when the temperature reaches 105 K. These findings indicate significant changes in the structure of $N_2O$ multilayers. We propose that a smaller TO−LO splitting could lead to overlapping of the negative and positive components, thus yielding a single positive band. At temperatures higher than 105 K, multilayer $N_2O$ molecules desorb completely and only the typical absorption doublet originating from the $N_2O$ monolayer remains.

Figure 9 shows the corresponding temperature resolved IRRAS data recorded with s polarized light. Overall, the spectral evolution is in line with the observation in the p polarized IR results (Figure 8). We note that the rather broad "positive" features in the spectra at 85−100 K should be related to the temperature induced background changes.

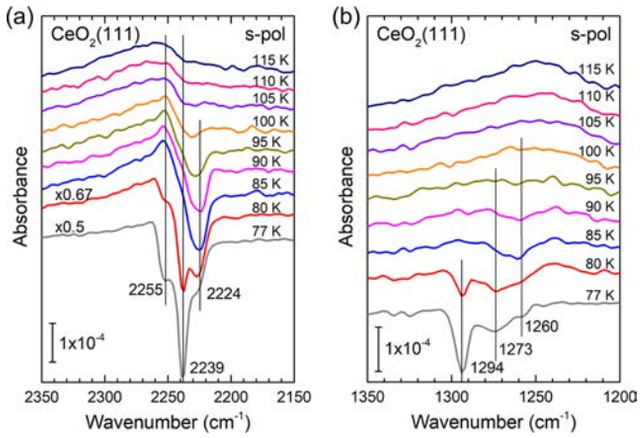


**Figure 9.** IRRA spectrum recorded directly after exposing the oxidized $CeO_2(111)$ to 5 L $N_2O$ at 77 K with s polarized light (lowest trace) and then heating gradually up to the indicated temperatures.

**3.5. NEXAFS and VB-PES.** We have also conducted NEXAFS and VB PES measurements for this system. The N K edge NEXAFS spectrum for the reduced $CeO_{2-x}(111)$ surface exposed to 50 L of $N_2O$ at 120 K and the spectral evolution over time are shown in Figure 10a. The acquisition of each spectrum took 3 min. The N K edge spectra show two intense resonances, which are assigned to the transition from the 1s orbitals of the terminal and central nitrogen atom, respectively, into the first unoccupied molecular orbital ($3\pi^*$).[72] Both resonances decrease in intensity during the measurements, which could be due to photoinduced desorption and/or decomposition of the $N_2O$ adsorbates. To further probe into this, an additional normal emission VB photoelectron spectrum was recorded after the NEXAFS measurements and compared with the VB photoelectron spectrum for the clean $CeO_{2-x}(111)$ sample. Upon reduction (i.e., oxygen vacancy formation), excess electrons would be left behind, which are localized in Ce 4f states. Thus, the intensity of the Ce 4f peak is directly related to the oxidation state of cerium cations at the surface.[73] If reoxidation of the reduced $CeO_{2-x}(111)$ surface occurs, the intensity of the Ce 4f peak is expected to decrease with a concomitant change in the shape of the O 2p peak. After exposure to $N_2O$, almost no change in the O 2p peak but a small decrease in intensity of the Ce 4f peak is observed in the VB photoelectron spectra (see Figure 10b), indicating that only a small fraction of the adsorbed $N_2O$ has had a dissociative interaction (N−O bond cession) with the surface under X ray irradiation during measurements, while the majority of the $N_2O$ species are desorbed from the surface.

NEXAFS and VB photoelectron spectroscopy measurements were also conducted for the reduced $CeO_{2-x}(110)$ surfaces. The photoinduced desorption and/or decomposition process is much faster and is already completed within the time of recording the first N K edge spectrum (see Figure S5a). From the comparison of the VB photoelectron spectra before and after exposure to $N_2O$, one can see that more $N_2O$ species are decomposed on reduced $CeO_{2-x}(110)$ during measurements and the O left behind reoxidizes the $CeO_{2-x}(110)$ to a greater extent than ceria (111) (see Figure S5b).

Reference experiments were also carried out for ceria powders (Nanophase Technologies). The N K edge NEXAFS spectra of the reduced ceria powders exposed to 50 L of $N_2O$ at 120 K and the evolution of the spectrum with time are

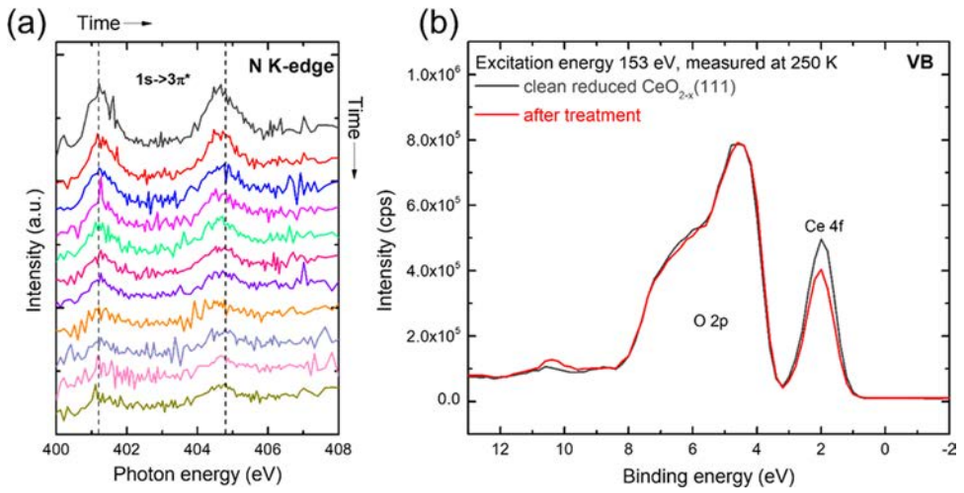


**Figure 10.** (a) Evolution of N K edge NEXAFS spectra measured on reduced $CeO_{2-x}$(111) after dosing of 50 L $N_2O$ at 120 K. (b) Normal emission VB photoelectron spectra of freshly prepared reduced $CeO_{2-x}$(111) and $CeO_{2-x}$(111) after completion of one $N_2O$ adsorption–desorption (and decomposition) cycle.

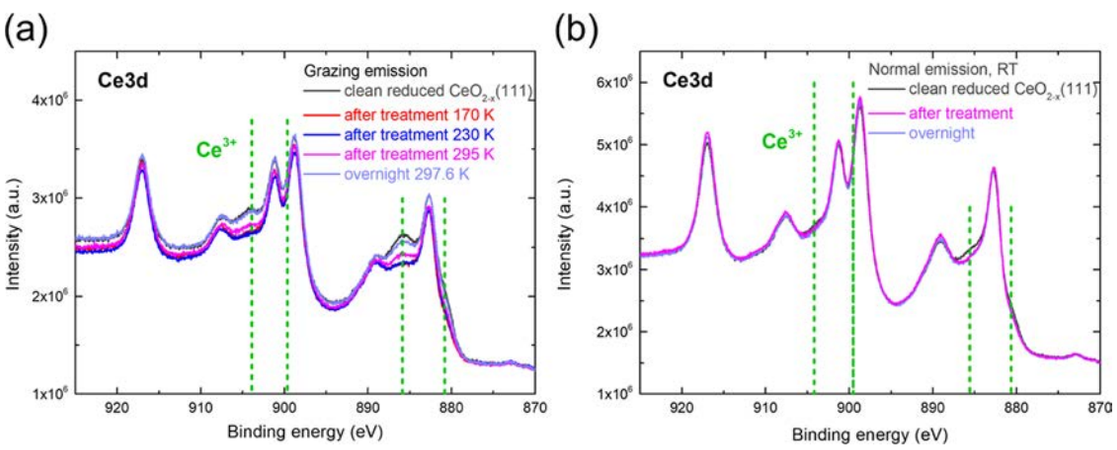


**Figure 11.** (a) Grazing emission XP spectra of freshly prepared reduced $CeO_{2-x}$(111) and $CeO_{2-x}$(111) warmed up to indicated temperatures after completion of one $N_2O$ adsorption–desorption cycle. (b) Normal emission XP spectra of freshly prepared reduced $CeO_{2-x}$(111) and $CeO_{2-x}$(111) after completion of one $N_2O$ adsorption–desorption (and decomposition) cycle at room temperature.

shown in Figure S6a. Similarly, the intensities of the $N_t$ and $N_c$ $\pi^*$ resonances also decrease during measurements. However, only a very small decrease of the Ce 4f peak was detected in the VB photoelectron spectrum after completion of one $N_2O$ adsorption–desorption (and decomposition) cycle compared to the clean reduced ceria powders (see Figure S6b). This indicates that most of the $N_2O$ species are desorbed from the surface during the measurements, and only a small fraction of $N_2O$ species is decomposed under X ray irradiation, which is in agreement with the results of the reduced $CeO_{2-x}$(111) single crystal surfaces. This in line with expectations, as ceria powders predominantly expose the most stable (111) facets.[74]

Figure 11 shows grazing and normal emission XP spectra of $CeO_{2-x}$(111) before and after completion of one $N_2O$ adsorption–desorption (and decomposition) cycle, respec tively. Clearly, there are more $Ce^{3+}$ cations (associated with oxygen vacancies, $O_v$) in the surface layers (grazing). In Figure 11a, the $Ce^{3+}$ concentration decreases dramatically after the $N_2O$ cycle, as shown by the XP spectrum measured at 170 K. This reveals that the $N_2O$ molecules dissociate on the surface and the O atoms left behind reoxidize the reduced $CeO_{2-x}$(111) sample. The Ce 3d XP spectrum does not change markedly when the sample temperature increases to 230 K. As the sample temperature is further raised up to 295 K, the $Ce^{3+}$ concentration increases to some extent. For the sample stored overnight in the UHV chamber, the $Ce^{3+}$ concentration increases significantly and is only slightly lower than that of the original clean reduced $CeO_{2-x}$(111) surface, suggesting that the O atoms diffuse into the bulk from the surface layers. The diffusion coefficient of oxygen anions in $CeO_2$ single crystal, $D_{diff}$, and the corresponding activation energy, $E_a$, have been computed and plotted previously, largely at high temperatures.[75,76] Assuming that the linear relationship between $Ln(O_2)$ and the reciprocal temperature holds to 300 K, the $D_{diff}$ of $O^{2-}$ in the $CeO_2$ single crystal is about $10^{-5}$ Å$^2$ $s^{-1}$. In Figure 11b, the normal emission Ce 3d XP spectrum of $CeO_{2-x}$(111) after the $N_2O$ cycle is nearly identical to that of $CeO_{2-x}$(111) stored overnight in the UHV chamber. This indicates that the O diffusion distance is in the range of the probing depth of the normal emission XPS. These two spectra show only a slight increase in $Ce^{3+}$ concentration compared to the clean reduced $CeO_{2-x}$(111) surfaces.

Finally, we would like to mention that the photoexcitation energy used here is below the work function (typically around

4.5 eV for ceria)[77] and thus leads to electron−hole pair excitations while the x rays lead to electron emission and these photoelectrons (primary and secondary) are responsible for the damage.

**3.6. Photoexcitation of $N_2O$ on $CeO_2(111)$ and $CeO_2(110)$ Surfaces in UHV.** To further gauge the extent of photostimulated surface reactions, previous experiments for $N_2O$ adsorption and photoreaction over $CeO_2(111)$ and $CeO_2(110)$ single crystals at 120 K[15] were further analyzed (see Figure S7). Figure 12 presents a plot of the $Ln(C_o/C_t)$ as

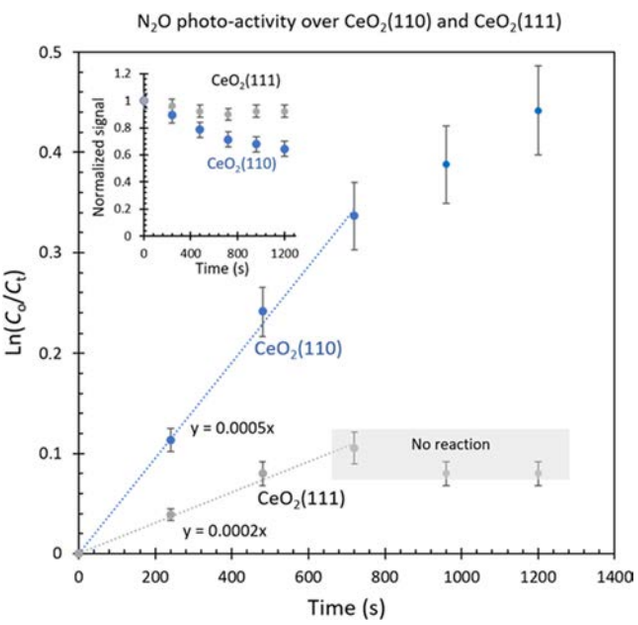


**Figure 12.** Extraction of photoreaction pseudo first order rate constants for $CeO_2(110)$ and $CeO_2(111)$ surfaces saturated with $N_2O$ at 120 K and excited with a 365 nm LED UV lamp with a light flux of $9 \times 10^{14}$ h$\nu$ cm$^{-2}$ s$^{-1}$; the surface area of each crystal is 1 cm$^2$.

a function of UV irradiation (365 nm, 3.40 eV) time on both surfaces, where $C_0$ and $C_t$ are the normalized IR signal of adsorbed $N_2O$ at time zero and time $t$, respectively. It is, however, important to mention that the reaction is not conducted in a dynamic mode but with a saturated surface with $N_2O$ prior to excitation. In other words, each site has seen the reactant only once and therefore while it is a true measure of the surface reactivity, it is not a catalytic reaction (in which, by definition, each surface site should be used more than once). On $CeO_2(111)$ there is a weak reaction that stops after about 10 min. A considerable surface coverage is still present (90% or so) once the reaction has stopped; it is therefore clear that the surface is not active for the reaction and most likely the weak decrease in the signal, initially, is due to some irreversible oxidation of minor surface defects by a photostimulated N−O bond dissociation. The situation is different for the (110) surface. The initial reaction cross section $A$ (cm$^2$) (where $A = k/F$, $F$ is the light flux, and $k$ is the pseudo first order rate constant in s$^{-1}$) is about $5 \times 10^{-19}$ cm$^2$. Because the reaction did not stop (although a slight change in the slope is noticed after about 10 min), it is highly likely that this cross is a measure of its activity, assuming that the rate is zero order with respect to the surface coverage. It is therefore clear that there is a relationship between the surface termination and the photoreaction cross section. Reasons for this observed anisotropy have been discussed before.[15,78] As such, anisotropy in the photoreaction on semiconductor surfaces is a well established concept although mostly in surface[79−81] and materials science[82] studies rather than in catalysis. The most common example is the anisotropic metal ion reduction on selective facets of $TiO_2$ single crystal surfaces[83] and $SrTiO_3$ nanocubes,[84] although some work on photocatalytic decom position pointed out to such a structure sensitivity[85] (anisotropy in reaction rates). In the case of $CeO_2$, two electronic/structural effects may be invoked for this phenom enon. First, it appears that the O 2p−Ce 4f gap of the (110) surface is smaller by up to 0.6 eV when compared to that of the (111) surface,[86,87] thus allowing more light to be absorbed. Second, it has been seen that $Ce^{3+}$ cations are easier to be formed on $CeO_2(110)$ when compared to $CeO_2(111)$.[88] While the presence of reduced states would decrease (not increase) the likelihood of excited electrons to be present (electrostatic repulsion), it induces considerable structural changes in the case of $CeO_2$ (lattice expansion among others).[89] Kinetic modeling of hopping polaron rates from the bulk to the surface as well as from different sites on the surfaces of $CeO_2(111)$ and $CeO_2(110)$ were studied by others in an attempt to understand the causes for this anisotropic effect.[78] It was found that the activation energy for polaron hopping from the bulk to the surface along the reduced $CeO_2(111)$ was larger by 0.25 eV than that on reduced $CeO_2(110)$: 0.72 and 0.47 eV, respectively. This in turn would affect the reaction steps of $N_2O$ decomposition, in particular, those related to electron transfer to the oxygen atom of the $N_2O$−Ce adsorbed complex, which is the initial step of the overall reaction ($N_2O + h\nu \rightarrow N_2 + 1/2\ O_2$).

## 4. CONCLUSIONS

A systematic study of the adsorption of $N_2O$ on monocrystal line $CeO_2(111)$ surfaces by polarization resolved IRRAS complemented by core level (XPS Ce 3d and NEXAFS) and valence band (Ce 4f) spectroscopy as well as DFT+U calculations was conducted. The IRRAS results at 110 K show that the $\nu_{as}$(NNO), asymmetric stretching vibration, of adsorbed $N_2O$ exhibits band splitting at relatively low $N_2O$ coverage in p polarized spectra. Such band splitting is attributed to polarization dependent shifts of the absorption bands. The temperature dependent IRRAS data reveal that $N_2O$ is more strongly bound to the reduced ceria (111) surface compared to the oxidized one. The extracted desorption energy for the stoichiometric surface (0.34 eV) was found to be closer to the adsorption energy computed using DFT+U (0.25−0.28 eV); reduced ceria (111) showed a larger desorption energy (0.37 eV). In synchrotron based NEXAFS and VB PES measurements, X ray induced decomposition of $N_2O$ on reduced ceria (111) surfaces occurred. However, the decomposition rate is much slower than that on reduced ceria (110) surfaces. These findings are in line with the observation of facet dependent (structure effect) photoreactivity of ceria for the decomposition of $N_2O$ under UV irradiation from which we have extracted the cross sections to be $5 \times 10^{-19}$ cm$^2$ for the (110) surface. The reason for the observed higher activity, in this work, might be linked to preferential hopping of polarons from the bulk to the surface for $CeO_2(110)$ when compared to that of $CeO_2(111)$, observed by others, which is in this case necessary to interact with the atoms of adsorbed $N_2O$(a) to initiate the dissociation reaction.

## AUTHOR INFORMATION


### Corresponding Authors

**Chengwu Yang** − *School of Space and Environment, Beihang University, Beijing 100191, China; Institute of Functional Interfaces, Karlsruhe Institute of Technology, 76344 Karlsruhe, Germany*; Email: yangcw@buaa.edu.cn

**Christof Wöll** − *Institute of Functional Interfaces, Karlsruhe Institute of Technology, 76344 Karlsruhe, Germany;* orcid.org/0000 0003 1078 3304; Email: christof.woell@kit.edu

### Authors

**Yunjun Cao** − *Lehrstuhl für Physikalische Chemie I, Ruhr Universität Bochum, 44801 Bochum, Germany*

**Philipp N. Plessow** − *Institute of Catalysis Research and Technology, Karlsruhe Institute of Technology, 76344 Karlsruhe, Germany;* orcid.org/0000 0001 9913 4049

**Jia Wang** − *School of Space and Environment, Beihang University, Beijing 100191, China*

**Alexei Nefedov** − *Institute of Functional Interfaces, Karlsruhe Institute of Technology, 76344 Karlsruhe, Germany;* orcid.org/0000 0003 2771 6386

**Stefan Heissler** − *Institute of Functional Interfaces, Karlsruhe Institute of Technology, 76344 Karlsruhe, Germany*

**Felix Studt** − *Institute of Catalysis Research and Technology, Karlsruhe Institute of Technology, 76344 Karlsruhe, Germany;* orcid.org/0000 0001 6841 4232

**Yuemin Wang** − *Institute of Functional Interfaces, Karlsruhe Institute of Technology, 76344 Karlsruhe, Germany;* orcid.org/0000 0002 9963 5473

**Hicham Idriss** − *Institute of Functional Interfaces, Karlsruhe Institute of Technology, 76344 Karlsruhe, Germany;* orcid.org/0000 0001 8614 7019

**Thomas G. Mayerhöfer** − *Leibniz Institute of Photonic Technology (IPHT), D 07745 Jena, Germany; Institute of Physical Chemistry, and Abbe Center of Photonics, Friedrich Schiller University, D 07743 Jena, Germany;* orcid.org/0000 0001 9396 7365


### Notes

The authors declare no competing financial interest.

## ACKNOWLEDGMENTS


This work was supported by the National Natural Science Foundation of China (21902005) and the Deutsche Forschungsgemeinschaft (DFG, German Research Foundation)—Project ID 426888090—SFB 1441. The authors want to thank HZB for the allocation of synchrotron radiation beamtime at BESSY II.


## REFERENCES


(1) Gandhi, H. S.; Piken, A. G.; Shelef, M.; Delosh, R. G. Laboratory evaluation of three way catalysts. *SAE Tech. Pap. Ser.* **1976**, *55*, No. 760201.

(2) Trovarelli, A.; Fornasiero, P. *Catalysis by Ceria and Related Materials*; 2nd ed.; Catalytic Science Series; Imperial College Press:London, United Kingdom, 2013; Vol. *12*.

(3) Montini, T.; Melchionna, M.; Monai, M.; Fornasiero, P. Fundamentals and catalytic applications of $CeO_2$ based materials. *Chem. Rev.* **2016**, *116*, 5987−6041.

(4) Doornkamp, C.; Ponec, V. The universal character of the Mars and Van Krevelen mechanism. *J. Mol. Catal. A: Chem.* **2000**, *162*, 19−32.

(5) Khan, M. M.; Ansari, S. A.; Pradhan, D.; Han, D. H.; Lee, J.; Cho, M. H. Defect induced band gap narrowed CeO2 nanostructures for visible light activities. *Ind. Eng. Chem. Res.* **2014**, *53*, 9754−9763.

(6) Hezam, A.; Namratha, K.; Drmosh, Q. A.; Ponnamma, D.; Wang, J.; Prasad, S.; Ahamed, M.; Cheng, C.; Byrappa, K. $CeO_2$ nanostructures enriched with oxygen vacancies for photocatalytic $CO_2$ reduction. *ACS Appl. Nano Mater.* **2020**, *3*, 138−148.

(7) Liyanage, A. D.; Perera, S. D.; Tan, K.; Chabal, Y.; Balkus, K. J. Synthesis, characterization, and photocatalytic activity of Y doped $CeO_2$ nanorods. *ACS Catal.* **2014**, *4*, 577−584.

(8) Lei, W.; Zhang, T.; Gu, L.; Liu, P.; Rodriguez, J. A.; Liu, G.; Liu, M. Surface structure sensitivity of $CeO_2$ nanocrystals in photocatalysis and enhancing the reactivity with nanogold. *ACS Catal.* **2015**, *5*, 4385−4393.

(9) Li, P.; Zhou, Y.; Zhao, Z.; Xu, Q.; Wang, X.; Xiao, M.; Zou, Z. Hexahedron prism anchored octahedronal $CeO_2$: Crystal facet based homojunction promoting efficient solar fuel synthesis. *J. Am. Chem. Soc.* **2015**, *137*, 9547−9550.

(10) Wuilloud, E.; Delley, B.; Schneider, W. D.; Baer, Y. Spectroscopic evidence for localized and extended *f* symmetry states in $CeO_2$. *Phys. Rev. Lett.* **1984**, *53*, 202−205.

(11) Pfau, A.; Schierbaum, K. D. The electronic structure of stoichiometric and reduced $CeO_2$ surfaces: an XPS, UPS and HREELS study. *Surf. Sci.* **1994**, *321*, 71−80.

(12) Mullins, D. R.; Overbury, S. H.; Huntley, D. R. Electron spectroscopy of single crystal and polycrystalline cerium oxide surfaces. *Surf. Sci.* **1998**, *409*, 307−319.

(13) Castleton, C. W. M.; Kullgren, J.; Hermansson, K. Tuning LDA +U for electron localization and structure at oxygen vacancies in ceria. *J. Chem. Phys.* **2007**, *127*, No. 244704.

(14) Shao, X.; Jerratsch, J. F.; Nilius, N.; Freund, H. J. Probing the 4f states of ceria by tunneling spectroscopy. *Phys. Chem. Chem. Phys.* **2011**, *13*, 12646−12651.

(15) Yang, C.; Yu, X.; Pleßow, P. N.; Heißler, S.; Weidler, P. G.; Nefedov, A.; Studt, F.; Wang, Y.; Wöll, C. Rendering photoreactivity to ceria: The role of defects. *Angew. Chem., Int. Ed.* **2017**, *56*, 14301−14305.

(16) Xu, M.; Gao, Y.; Moreno, E. M.; Kunst, M.; Muhler, M.; Wang, Y.; Idriss, H.; Wöll, C. Photocatalytic activity of bulk $TiO_2$ anatase and rutile single crystals using infrared absorption spectroscopy. *Phys. Rev. Lett.* **2011**, *106*, No. 138302.

(17) Schwarz, M.; Schuschke, C.; Silva, T. N.; Mohr, S.; Waidhas, F.; Brummel, O.; Libuda, J. A simple high intensity UV photon source for photochemical studies in UHV: Application to the photo conversion of norbornadiene to quadricyclane. *Rev. Sci. Instrum.* **2019**, *90*, No. 024105.

(18) Ravishankara, A. R.; Daniel John, S.; Portmann Robert, W. Nitrous oxide ($N_2O$): The dominant ozone depleting substance emitted in the 21st century. *Science* **2009**, *326*, 123−125.

(19) Ciais, P.; Sabine, C.; Bala, G.; Bopp, L.; Brovkin, V.; Canadell, J.; Chhabra, A.; DeFries, R.; Galloway, J.; Heimann, M. Carbon and other Biogeochemical Cycles. In *Climate Change 2013: The Physical Science Basis. Contribution of Working Group I to the Fifth Assessment Report of the Intergovernmental Panel on Climate Change*; Cambridge University Press: Cambridge, United Kingdom and New York, USA, 2014; Chapter 6, pp 465−570.

(20) Ji, Q.; Buitenhuis, E.; Suntharalingam, P.; Sarmiento, J. L.; Ward, B. B. Global nitrous oxide production determined by oxygen sensitivity of nitrification and denitrification. *Global Biogeochem. Cycles* **2018**, *32*, 1790−1802.
(21) Thompson, R. L.; Lassaletta, L.; Patra, P. K.; Wilson, C.; Wells, K. C.; Gressent, A.; Koffi, E. N.; Chipperfield, M. P.; Winiwarter, W.; Davidson, E. A.; et al. Acceleration of global $N_2O$ emissions seen from two decades of atmospheric inversion. *Nat. Clim. Change* **2019**, *9*, 993−998.
(22) Solomon, S.; Alcamo, J.; Ravishankara, A. R. Unfinished business after five decades of ozone layer science and policy. *Nat. Commun.* **2020**, *11*, No. 4272.
(23) Tian, H.; Xu, R.; Canadell, J. G.; Thompson, R. L.; Winiwarter, W.; Suntharalingam, P.; Davidson, E. A.; Ciais, P.; Jackson, R. B.; Janssens Maenhout, G.; et al. A comprehensive quantification of global nitrous oxide sources and sinks. *Nature* **2020**, *586*, 248−256.
(24) García García, A.; Bueno López, A. Interaction of nitrogen oxides with ceria based materials. In *Catalysis by Ceria and Related Materials*; 2nd ed.; Catalytic Science Series; Imperial College Press: London, United Kingdom, 2013; Chapter 4, Vol. *12*, pp 223−246.
(25) Konsolakis, M. Recent advances on nitrous oxide ($N_2O$) decomposition over non noble metal oxide catalysts: Catalytic performance, mechanistic considerations, and surface chemistry aspects. *ACS Catal.* **2015**, *5*, 6397−6421.
(26) Giese, P.; Kirsch, H.; Wolf, M.; Frischkorn, C. Reduction of $N_2O$ on MgO/Ag(100) via UV photoinduced trapped electrons. *J. Phys. Chem. C* **2011**, *115*, 10012−10018.
(27) Kim, K. H.; Watanabe, K.; Menzel, D.; Freund, H. J. UV photo dissociation and photodesorption of $N_2O$ on Ag(111). *J. Phys.: Condens. Matter* **2010**, *22*, No. 084012.
(28) Rusu, C. N.; Yates, J. T. $N_2O$ adsorption and photochemistry on high area $TiO_2$ powder. *J. Phys. Chem. B* **2001**, *105*, 2596−2603.
(29) Papanikolaou, K. G.; Stamatakis, M. The catalytic decom position of nitrous oxide and the NO + CO reaction over Ni/Cu dilute and single atom alloy surfaces: first principles microkinetic modelling. *Catal. Sci. Technol.* **2021**, *11*, 3681−3696.
(30) Kočí, K.; Reli, M.; Troppová, I.; Šihor, M.; Bajcarová, T.; Ritz, M.; Pavlovský, J.; Praus, P. Photocatalytic decomposition of $N_2O$ by using nanostructured graphitic carbon nitride/zinc oxide photo catalysts immobilized on foam. *Catalysts* **2019**, *9*, 735.
(31) Kočí, K.; Krejčíková, S.; Šolcová, O.; Obalová, L. Photocatalytic decomposition of $N_2O$ on Ag $TiO_2$. *Catal. Today* **2012**, *191*, 134−137.
(32) Zhu, J.; Su, Y.; Chai, J.; Muravev, V.; Kosinov, N.; Hensen, E. J. M. Mechanism and nature of active sites for methanol synthesis from $CO/CO_2$ on $Cu/CeO_2$. *ACS Catal.* **2020**, *10*, 11532−11544.
(33) Wang, Y.; Wöll, C. IR spectroscopic investigations of chemical and photochemical reactions on metal oxides: bridging the materials gap. *Chem. Soc. Rev.* **2017**, *46*, 1875−1932.
(34) Yang, C.; Yin, L. L.; Bebensee, F.; Buchholz, M.; Sezen, H.; Heissler, S.; Chen, J.; Nefedov, A.; Idriss, H.; Gong, X. Q.; et al. Chemical activity of oxygen vacancies on ceria: a combined experimental and theoretical study on $CeO_2(111)$. *Phys. Chem. Chem. Phys.* **2014**, *16*, 24165−24168.
(35) Yang, C.; Bebensee, F.; Nefedov, A.; Wöll, C.; Kropp, T.; Komissarov, L.; Penschke, C.; Moerer, R.; Paier, J.; Sauer, J. Methanol adsorption on monocrystalline ceria surfaces. *J. Catal.* **2016**, *336*, 116−125.
(36) Yang, C.; Yu, X.; Heißler, S.; Nefedov, A.; Colussi, S.; Llorca, J.; Trovarelli, A.; Wang, Y.; Wöll, C. Surface faceting and reconstruction of ceria nanoparticles. *Angew. Chem., Int. Ed.* **2017**, *56*, 375−379.
(37) Kresse, G.; Joubert, D. From ultrasoft pseudopotentials to the projector augmented wave method. *Phys. Rev. B* **1999**, *59*, 1758−1775.
(38) Kresse, G.; Furthmüller, J. Efficient iterative schemes for ab initio total energy calculations using a plane wave basis set. *Phys. Rev. B* **1996**, *54*, 11169−11186.
(39) Perdew, J. P.; Burke, K.; Ernzerhof, M. Generalized gradient approximation made simple. *Phys. Rev. Lett.* **1996**, *77*, 3865−3868.
(40) Perdew, J. P.; Burke, K.; Ernzerhof, M. Generalized gradient approximation made simple [Phys. Rev. Lett. 77, 3865 (1996)]. *Phys. Rev. Lett.* **1997**, *78*, 1396.
(41) Grimme, S.; Antony, J.; Ehrlich, S.; Krieg, H. A consistent and accurate ab initio parametrization of density functional dispersion correction (DFT D) for the 94 elements H Pu. *J. Chem. Phys.* **2010**, *132*, No. 154104.
(42) Dudarev, S. L.; Botton, G. A.; Savrasov, S. Y.; Humphreys, C. J.; Sutton, A. P. Electron energy loss spectra and the structural stability of nickel oxide: An LSDA+U study. *Phys. Rev. B* **1998**, *57*, 1505−1509.
(43) Liechtenstein, A. I.; Anisimov, V. I.; Zaanen, J. Density functional theory and strong interactions: Orbital ordering in Mott Hubbard insulators. *Phys. Rev. B* **1995**, *52*, R5467−R5470.
(44) Anisimov, V. I.; Aryasetiawan, F.; Lichtenstein, A. I. First principles calculations of the electronic structure and spectra of strongly correlated systems: the LDA+*U* method. *J. Phys.: Condens. Matter* **1997**, *9*, 767−808.
(45) Anisimov, V. I.; Zaanen, J.; Andersen, O. K. Band theory and Mott insulators: Hubbard U instead of Stoner I. *Phys. Rev. B* **1991**, *44*, 943−954.
(46) Nefedov, A.; Wöll, C. Advanced applications of NEXAFS spectroscopy for functionalized surfaces. In *Surface Science Techniques*; Springer Series in Surface Sciences; Springer: Berlin, Heidelberg, Germany, 2013; Vol. *51*, pp 277−303.
(47) Chabal, Y. J. Surface infrared spectroscopy. *Surf. Sci. Rep.* **1988**, *8*, 211−357.
(48) Richter, L. J.; Buntin, S. A.; Chu, P. M.; Cavanagh, R. R. Adsorption and photodecomposition of $Mo(CO)_6$ on Si(111) 7×7: An infrared reflection absorption spectroscopy study. *J. Chem. Phys.* **1994**, *100*, 3187−3200.
(49) Yang, C.; Wöll, C. IR spectroscopy applied to metal oxide surfaces: adsorbate vibrations and beyond. *Adv. Phys.: X* **2017**, *2*, 373−408.
(50) Müller, C. Physisorption of CO and $N_2O$ on ceria surfaces. Doctoral Thesis, Acta Universitatis Upsaliensis: Uppsala, 2009.
(51) Wood, B. R.; Reimer, J. A.; Bell, A. T. Studies of $N_2O$ adsorption and decomposition on Fe ZSM 5. *J. Catal.* **2002**, *209*, 151−158.
(52) Borello, E.; Cerruti, L.; Ghiotti, G.; Guglielminotti, E. Surface complexes of nitrous oxide adsorbed on $\alpha$ $Cr_2O_3$. *Inorg. Chim. Acta* **1972**, *6*, 45−48.
(53) Tolman, W. B. Binding and activation of $N_2O$ at transition metal centers: Recent mechanistic insights. *Angew. Chem., Int. Ed.* **2010**, *49*, 1018−1024.
(54) Buchholz, M.; Yu, X.; Yang, C.; Heißler, S.; Nefedov, A.; Wang, Y.; Wöll, C. IR spectroscopy of CO adsorption on mixed terminated ZnO surfaces. *Surf. Sci.* **2016**, *652*, 247−252.
(55) Yang, C.; Yu, X.; Heißler, S.; Weidler, P. G.; Nefedov, A.; Wang, Y.; Wöll, C.; Kropp, T.; Paier, J.; Sauer, J. $O_2$ activation on ceria catalysts—The importance of substrate crystallographic orientation. *Angew. Chem., Int. Ed.* **2017**, *56*, 16399−16404.
(56) Ganduglia Pirovano, M. V.; Da Silva, J. L. F.; Sauer, J. Density functional calculations of the structure of near surface oxygen vacancies and electron localization on $CeO_2(111)$. *Phys. Rev. Lett.* **2009**, *102*, No. 026101.
(57) Murgida, G. E.; Ganduglia Pirovano, M. V. Evidence for subsurface ordering of oxygen vacancies on the reduced $CeO_2(111)$ surface using density functional and statistical calculations. *Phys. Rev. Lett.* **2013**, *110*, No. 246101.
(58) Han, Z. K.; Yang, Y. Z.; Zhu, B.; Ganduglia Pirovano, M. V.; Gao, Y. Unraveling the oxygen vacancy structures at the reduced $CeO_2(111)$ surface. *Phys. Rev. Mater.* **2018**, *2*, No. 035802.
(59) Jerratsch, J. F.; Shao, X.; Nilius, N.; Freund, H. J.; Popa, C.; Ganduglia Pirovano, M. V.; Burow, A. M.; Sauer, J. Electron localization in defective ceria films: A study with scanning tunneling microscopy and density functional theory. *Phys. Rev. Lett.* **2011**, *106*, No. 246801.

(60) Torbrügge, S.; Reichling, M.; Ishiyama, A.; Morita, S.; Custance, Ó. Evidence of subsurface oxygen vacancy ordering on reduced $CeO_2(111)$. *Phys. Rev. Lett.* **2007**, *99*, No. 056101.
(61) Tuller, H. L.; Nowick, A. S. Small polaron electron transport in reduced $CeO_2$ single crystals. *J. Phys. Chem. Solids* **1977**, *38*, 859−867.
(62) Naik, I. K.; Tien, T. Y. Small polaron mobility in non stoichiometric cerium dioxide. *J. Phys. Chem. Solids* **1978**, *39*, 311−315.
(63) Castleton, C. W. M.; Lee, A.; Kullgren, J. Benchmarking density functional theory functionals for polarons in oxides: Properties of $CeO_2$. *J. Phys. Chem. C* **2019**, *123*, 5164−5175.
(64) Zhang, D.; Han, Z. K.; Murgida, G. E.; Ganduglia Pirovano, M. V.; Gao, Y. Oxygen vacancy dynamics and entanglement with polaron hopping at the reduced $CeO_2(111)$ surface. *Phys. Rev. Lett.* **2019**, *122*, No. 096101.
(65) Müller, C.; Hermansson, K.; Paulus, B. Electron correlation contribution to the $N_2O$/ceria(111) interaction. *Chem. Phys.* **2009**, *362*, 91−96.
(66) Weiss, H. The monolayer $N_2O$/NaCl(001): An FTIRS, LEED and HAS study. *Surf. Sci.* **1995**, *331 333*, 1453−1459.
(67) Heidberg, J.; Redlich, B. The adsorption of $CO_2$ and $N_2O$ on the MgO(001) single crystal surface: a comparative PIRSS and LEED study. *Surf. Sci.* **1996**, *368*, 140−146.
(68) Yang, C.; Wang, W.; Nefedov, A.; Wang, Y.; Mayerhöfer, T. G.; Wöll, C. Polarization dependent vibrational shifts on dielectric substrates. *Phys. Chem. Chem. Phys.* **2020**, *22*, 17129−17133.
(69) Berreman, D. W. Infrared absorption at longitudinal optic frequency in cubic crystal films. *Phys. Rev.* **1963**, *130*, 2193−2198.
(70) Cassidy, A.; Jørgensen, M. R. V.; Rosu Finsen, A.; Lasne, J.; Jørgensen, J. H.; Glavic, A.; Lauter, V.; Iversen, B. B.; McCoustra, M. R. S.; Field, D. Dipole oriented molecular solids can undergo a phase change and still maintain electrical polarization. *J. Phys. Chem. C* **2016**, *120*, 24130−24136.
(71) Wöll, C. Structure and chemical properties of oxide nanoparticles determined by surface ligand IR spectroscopy. *ACS Catal.* **2020**, *10*, 168−176.
(72) Ceballos, G.; Wende, H.; Baberschke, K.; Arvanitis, D. Molecular geometry modifications upon adsorption for $N_2O$: N and O K edge NEXAFS. *Surf. Sci.* **2001**, *482−485*, 15−20.
(73) Yang, C.; Bebensee, F.; Chen, J.; Yu, X.; Nefedov, A.; Wöll, C. Carbon dioxide adsorption on $CeO_2(110)$: An XPS and NEXAFS study. *ChemPhysChem* **2017**, *18*, 1874−1880.
(74) Wang, R.; Mutinda, S. I. The dynamic shape of ceria nanoparticles. *Chem. Phys. Lett.* **2011**, *517*, 186−189.
(75) Ikuma, Y.; Kamiya, M.; Shimada, E. Nonstoichiometry and diffusion in ceria and ceria solid solutions. *Key Eng. Mater.* **2003**, *253*, 225−242.
(76) Sameshima, S.; Ono, H.; Higashi, K.; Sonoda, K.; Hirata, Y.; Ikuma, Y. Electrical conductivity and diffusion of oxygen ions in rare earth doped ceria. *J. Ceram. Soc. Jpn.* **2000**, *108*, 1060−1066.
(77) Wardenga, H. F.; Klein, A. Surface potentials of (111), (110) and (100) oriented CeO2 x thin films. *Appl. Surf. Sci.* **2016**, *377*, 1−8.
(78) Song, W.; Wang, L.; Gao, Y.; Deng, J.; Jing, M.; Zheng, H.; Liu, J.; Zhao, Z.; Gao, M.; Wei, Y. Unraveling the structure−sensitivity of the photocatalytic decomposition of $N_2O$ on $CeO_2$: a DFT+U study. *J. Mater. Chem. A* **2018**, *6*, 19241−19255.
(79) Morris Hotsenpiller, P. A.; Bolt, J. D.; Farneth, W. E.; Lowekamp, J. B.; Rohrer, G. S. Orientation dependence of photochemical reactions on $TiO_2$ surfaces. *J. Phys. Chem. B* **1998**, *102*, 3216−3226.
(80) Fang, F.; Liu, Y.; Sun, X.; Fu, C.; Prakash Bhoi, Y.; Xiong, W.; Huang, W. $TiO_2$ Facet dependent reconstruction and photocatalysis of $CuO_x/TiO_2$ photocatalysts in $CO_2$ photoreduction. *Appl. Surf. Sci.* **2021**, *564*, No. 150407.
(81) Li, R.; Zhang, F.; Wang, D.; Yang, J.; Li, M.; Zhu, J.; Zhou, X.; Han, H.; Li, C. Spatial separation of photogenerated electrons and holes among {010} and {110} crystal facets of $BiVO_4$. *Nat. Commun.* **2013**, *4*, No. 1432.
(82) Pisat, A. S.; Rohrer, G. S.; Salvador, P. A. Spatial selectivity of photodeposition reactions on polar surfaces of centrosymmetric ferroelastic $\gamma$ $WO_3$. *J. Mater. Chem. A* **2017**, *5*, 8261−8266.
(83) Lowekamp, J. B.; Rohrer, G. S.; Morris Hotsenpiller, P. A.; Bolt, J. D.; Farneth, W. E. Anisotropic photochemical reactivity of bulk $TiO_2$ crystals. *J. Phys. Chem. B* **1998**, *102*, 7323−7327.
(84) Giocondi, J. L.; Rohrer, G. S. Structure sensitivity of photochemical oxidation and reduction reactions on $SrTiO_3$ surfaces. *J. Am. Ceram. Soc.* **2003**, *86*, 1182−1189.
(85) Wilson, J. N.; Idriss, H. Structure sensitivity and photocatalytic reactions of semiconductors. Effect of the last layer atomic arrangement. *J. Am. Chem. Soc.* **2002**, *124*, 11284−11285.
(86) Skorodumova, N. V.; Baudin, M.; Hermansson, K. Surface properties of $CeO_2$ from first principles. *Phys. Rev. B* **2004**, *69*, No. 075401.
(87) Yang, Z.; Woo, T. K.; Baudin, M.; Hermansson, K. Atomic and electronic structure of unreduced and reduced $CeO_2$ surfaces: A first principles study. *J. Chem. Phys.* **2004**, *120*, 7741−7749.
(88) Choudhury, B.; Chetri, P.; Choudhury, A. Oxygen defects and formation of $Ce^{3+}$ affecting the photocatalytic performance of $CeO_2$ nanoparticles. *RSC Adv.* **2014**, *4*, 4663−4671.
(89) Hailstone, R. K.; DiFrancesco, A. G.; Leong, J. G.; Allston, T. D.; Reed, K. J. A study of lattice expansion in $CeO_2$ nanoparticles by transmission electron microscopy. *J. Phys. Chem. C* **2009**, *113*, 15155−15159.